physica status solidi b
www.pss-b.com

Parameter-Free Calculation for the Optical Bandgap Energies of InGaAlN

Takashi Matsuoka, Yoshiyuki Kawazoe, and Talgat M. Inerbaev*

The accurate prediction of bandgap energy E_g is crucial for the future development of semiconductors. Ab initio simulation studies have been undertaken to unravel the intricacies of compound semiconductors. However, traditional density functional theory estimates E_g to be mostly 30–50% smaller than experimental values. To reconcile these disparities, fitting parameters such as U have been employed, albeit at the expense of violating the virial theorem's essential conditions. In our pursuit of a more accurate approach, utilizing a computational method that adheres to virial's theorem without resorting to fitting parameters is proposed. Employing the self-consistent Green-function vertex (GW) approximation calculation, standard phenomenological results are built upon as an initial condition. This novel methodology successfully resolves the long-standing issue surrounding E_g of InN, a nitride semiconductor InGaAlN known for blue light-emitting diodes. The numerical results from our calculations demonstrate a remarkable alignment with experimental values across the entire $In_xGa_{1-x}N$ range, with an impressive accuracy of 0.1 eV. This innovative method holds promise for application to various semiconductors, serving as a potent tool for predicting new semiconductors with small E_g. This calculation method is also applied to E_g of $In_{1-x}Al_xN$ and $Ga_{1-x}Al_xN$.

1. Introduction

The proposal of wurtzite InGaAlN to allow the construction of a double heterostructure and the growth of single crystalline $In_xGa_{1-x}N$ as a blue-light emitter for the first time were reported in 1989.[1] Subsequently, the exploration of the optical and electronic properties in nitride semiconductors with a wurtzite structure has primarily centered around optical devices, specifically blue and white light-emitting diodes (LEDs).[2–4] The deployment of white LEDs has contributed to energy saving in solid-state lighting.[5] As anticipated from solid-state properties, there has been also notable progress in the development of electronic devices, including high electron mobility transistors (HEMTs) which were developed. Currently, $Ga_{1-x}Al_xN$/GaN HEMTs find widespread application in the base stations of fourth-generation cellular phones. Additionally, inverted HEMTs featuring the GaN/$Ga_{1-x}Al_xN$ structure, designed to operate at high speed, have been successfully fabricated.[6] In the automotive industry, there is a growing demand for vertical transistors characterized by high power and high breakdown voltage, particularly for the development of highly efficient inverters.

At the time of the first growth report, the optical bandgap energy, commonly referred to as "bandgap energy" (E_g), for $In_xGa_{1-x}N$ with x of up to 42% was documented.[1] This E_g information also led to the prediction that E_g of single-crystal InN would be significantly lower than the ≈2 eV measured from polycrystal.[7] In 2002, the successful growth of single-crystal InN was achieved using both MOVPE[8] and MBE,[9,10] confirming experimentally that its bandgap energy ranged from 0.7 to 0.8 eV. This breakthrough expanded the adaptable range of the long-wavelength side in InGaAlN, surpassing the previously believed orange range and extending into the infrared spectrum. Consequently, InGaAlN now demonstrates the capability to cover a wide wavelength range from UV to infrared.

Currently, there is still a lingering concern regarding the accuracy of E_g measurement. This uncertainty stems from the high conductivity of measured InN, where the Burnstein–Moss shift occurs due to the presence of electron filling the conduction band, resulting in an elevated bandgap energy.

For the future development of semiconductors, the prediction of the bandgap energy holds significant importance. Ab initio simulation studies have been pivotal in comprehending the

T. Matsuoka, Y. Kawazoe
New Industry Creation Hatchery Center
Tohoku University
6-6-10, Aoba, Aramaki, Aoba-ku, Sendai-shi, Miyagi 980-8579, Japan
E-mail: takashi.matsuoka.b6@tohoku.ac.jp

Y. Kawazoe
SRM Institute of Science and Technology
SRM Nagar, Kattankulathur, Kancheepuram District, Chennai, Tamil Nadu 603203, India

Y. Kawazoe
Suranaree University of Technology
111 University Avenue, Muang, Nakhon Ratchasima 30000, Thailand

T. M. Inerbaev
Vernadsky Institute of Geochemistry and Analytical Chemistry
Russian Academy of Science
119991 Moscow, Russia

T. M. Inerbaev
L.N. Gumilyov Eurasian National University
Satpayev 2, Astana 010008, Republic of Kazakhstan

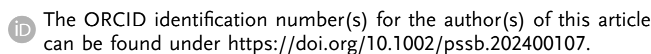
The ORCID identification number(s) for the author(s) of this article can be found under https://doi.org/10.1002/pssb.202400107.

© 2024 The Author(s). physica status solidi (b) basic solid state physics published by Wiley-VCH GmbH. This is an open access article under the terms of the Creative Commons Attribution License, which permits use, distribution and reproduction in any medium, provided the original work is properly cited.

DOI: 10.1002/pssb.202400107

 © 2024 The Author(s). physica status solidi (b) basic solid state physics published by Wiley-VCH GmbH

nature of the compound semiconductor. Numerous theoretical investigations have been published on $In_xGa_{1-x}N$. However, when applying the density-functional theory (DFT) with local-density approximation (LDA) or generalized-gradient approximation (GGA), the estimated bandgap energy is ≈50% smaller than the experimental values, and notably, it even becomes negative for InN.[11–13] Several attempts have been made using LDA + U or hybrid functional with parameter α. Although these methods are considered standard in present-day ab initio calculations, they incorporate phenomenological parameters to align with experimental observations. Consequently, they cannot be classified as exact ab initio calculation and lack the potential to predict new materials. Our efforts have been directed toward establishing a truly parameter-free ab initio method based on physics that satisfies all necessary conditions for many body electronic systems. Its calculation method is perfectly parameter-free different from the conventional calculation methods.

In this article, we initially delve into the historical progression of past calculation methods. Subsequently, we elucidate the accuracy of our method, based on the physical concept. As an illustrative application of our approach, we present the numerical results of the bandgap energy of $In_xGa_{1-x}N$, a pivotal material for device applications in nitride semiconductors. Finally, the obtained numerical results are demonstrated to align remarkably well with experimental data, affirming the reliability of our calculation method.

We have previously presented a comprehensive overview of our theoretical calculation method for determining bandgap energies in $In_xGa_{1-x}N$, along with the corresponding results (ref. [14]). In this article, we aim to delve deeper into the theory, elucidate its visual representation, and provide a more intricate explanation of the computational methods employed. In addition, calculation results of bandgap energies for $In_{1-x}Al_xN$ and $Ga_{1-x}Al_xN$, which are members of the same nitride semiconductor family as $In_xGa_{1-x}N$, are also shown. In the calculation of bandgap energy, the bandgap energy was obtained from the difference between the maximum energy of the valence band (valence band maximum, VBM) and the minimum energy of the conduction band (conduction band minimum, CBM). These values are essential for the design of devices using heterojunctions, so these values are also shown as figures.

2. Various Levels of Ab Initio Simulation Methods

2.1. Conventional Methods

DFT combined with LDA or GGA has been widely utilized to explore diverse electronic properties in post-transition metal (TM) compounds, encompassing both oxides and nitrides. However, it is noteworthy that these models are not applicable to very heavy atoms due to their nonrelativistic nature. Nevertheless, they prove to be effective in the analysis of TM compounds.

To address the many-body electronic problem through variational methods for wavefunctions, it becomes essential to employ 3^n variables, where n represents the number of electrons. Prof. Kohn ingeniously devised a method in 1964[15] to reduce the variables from 3^n to 3, utilizing electron charge density as the variable, a technique now known as DFT. This innovation significantly reduces the computational complexity associated with the many-body electronic problem, albeit with the limitation of being applicable primarily to the ground state.

Initially applied in the electron gas model, LDA assumes uniform electron distribution throughout the system, ignoring electron congregation at the nucleus position. Consequently, LDA, compared with reality, provides a coarse representation of the actual electron distribution in the atom. To address this, GGA with a first-order approximation slope emerged, aiming to correct for the increased electron density near the nucleus. While DFT serves as a comprehensive many-body theory, its fundamental applicability lies within the nondegenerate ground state.

When DFT is employed for the bandgap value estimation, a significant drawback emerges as it tends to seriously underestimate the bandgap energy, mostly in the 50–70% range for most post-TM compounds and up to 80% reduction in the case of ZnO. The underestimate occurs because DFT, being a ground-state theory, cannot accurately represent the conduction band. However, when the plane-wave expansion is diagonalized, the corresponding conduction band portion is identified and used to determine the bandgap energy.[16]

Although DFT struggles to estimate level energies above the Fermi level, the angular momentum of these levels aligns with the exact solution, and the band dispersion curves exhibit similar behavior. In certain cases, such as InN, DFT predicts a negative bandgap energy, implying metallic properties.[11–13] Similarly, for GaN, DFT calculation results in a notably underestimated bandgap value.[12,17] This extensional use of DFT for bandgap energy estimation, especially beyond its ground-state scope, is theoretically incorrect. To address excitation states, higher-level theoretical methods like Green-function vertex (GW) approximation are necessary. GW, a first-order perturbation term, introduces electron correlation into the Hartree–Fock calculation and is empirically known to enhance accuracy, even within the framework of DFT. Despite DFT incorporating some electron correlations, caution is warranted as the electron correlation is double counted. However, empirical evidence suggests an accuracy of ≈0.1 eV based on comparisons with experimental data.

Addressing the underestimation of the bandgap energy in post-TM compounds involves considering the onsite electron correlation energy U. This empirical treatment aims to account for the correlations of d-electrons, which contribute to an increase in the bandgap value. However, it is worth noting that the DFT + U method violates the virial theorem's necessary condition ($2T + V = 0$), where T represents kinetic energy and V potential energy. The virial theorem is a fundamental relation between kinetic and potential energy applicable in a steady state for a many-electron system interacting via Coulomb force with motion in a finite range.

DFT + U method also introduces nonphysical effects on other physical parameters. In DFT + U, the virial theorem does not hold. Lattice constants, for instance, are reduced, contributing to a widening of the bandgap. An alternative approach involves the use of hybrid functional schemes, which incorporate the exact term for the electron exchange energy from Hartree–Fock approximation. This method aims to improve the bandgap energy by accurately calculating the electron exchange energy, which DFT struggles with due to its incorporation into the kinetic energy term, among other factors. However, adjusting

© 2024 The Author(s). physica status solidi (b) basic solid state physics published by Wiley-VCH GmbH

15213951, 2025, 3, Downloaded from https://onlinelibrary.wiley.com/doi/10.1002/pssb.202400107 by L.N. Gumilyov Eurasian National University, Wiley Online Library on [18/09/2025]. See the Terms and Conditions (https://onlinelibrary.wiley.com/terms-and-conditions) on Wiley Online Library for rules of use; OA articles are governed by the applicable Creative Commons License

the fraction of the exact exchange energy for different post-TM compounds to match the bandgap energy remains a phenomenological treatment.[11,16]

Recent advancements in theoretical modeling methods enable the prediction of fundamental bandgap values with high accuracy, eliminating the need for parameters. This is achieved by combining DFT and the quasiparticle (QP) theory within the GW approximation for the exchange-correlation self-energy.[18] QP, in this context, represents the physical picture of an electron surrounded by other electrons, with DFT dealing with QPs rather than just electrons. The GW approximation incorporates the basic part of electron correlation, accounting for photon emission and absorption in the Hartree–Fock calculation, which lacks electron correlation. By considering QP corrections, this approach resolves the bandgap problem with an accuracy of about 0.1 eV.[19]

The first attempt to calculate the electronic properties of $In_xGa_{1-x}N$ ternary alloys without parameter was conducted using the LDA-1/2 method in ref. [20]. This method, based on the approximation of the half-filled conduction band,[21] treats the portion without electrons as a hole, yielding considerably accurate results. It approximately includes the self-energy of excitations in semiconductors and closely aligns with calculations using the GW method.

The many-body perturbation theory within the GW approach introduces a QP theory that addresses the limitations of LDA and GGA. This theoretical framework offers a more accurate description of the band structure, particularly for weakly correlated solids like GaN and InN. The GW approximation formally represents the initial term in an expansion of the nonlocal and energy-dependent self-energy in the screened Coulomb interaction.[22] The self-energy operator is described as follows

$$\Sigma(r, r' \in) = \frac{i}{4\pi} \int_{-\infty}^{\infty} e^{i\omega'\delta}\, G(r, r' \in +\omega')\, W(r, r')\, d\omega' \qquad (1)$$

where G is Green's function, W is the screened Coulomb interaction, and δ is infinitesimal. The calculation of self-energy necessitates both wave functions and corresponding eigenvalues. When these quantities are fixed to DFT results, it is commonly referred to as single-shot G_0W_0 calculations (0 denotes nonself-consistent calculations, utilizing DFT wavefunctions). The GW_0 and GW approximations involve iterative updates of eigenvalues in the computation of G and W, respectively. Achieving a complete update of electron wave-function orbitals can be accomplished through self-consistent GW (scGW) calculations. If the orbitals and eigenvalues are updated in both G and W, it is categorized as scGW approximation, whereas scGW0 involves updating orbitals and eigenvalues only in G calculations. Besides the level of self-consistency, the outcomes are influenced by initial conditions, specifically the method from which eigenvalues and orbitals are derived in GW calculations.

Extensive studies employing the GW method highlight that numerical results are highly sensitive to the initial structure's geometry and the choice of starting wave functions.[11,12,23–32] Therefore, utilizing source structures optimized with various functionals introduces variations in the numerical values of the bandgap. For instance, optimizing the wurtzite structure of GaN with GGA-Perdew–Burke–Ernzerhof (PBE) results in the bandgap ranging from 3.366 to 3.847 eV with LDA optimization.[32]

The selection of the initial wave function in GW calculations is a critical factor. Kang et al.[16] conducted comprehensive tests on various levels of self-consistency and starting conditions to identify the most suitable GW calculation scheme for accurately describing the bandgap value in post-TM oxides. Their findings revealed that the GW_0 scheme with GGA + U as the DFT functional consistently produced optimal results across all aspects of band structures. In the specific case of ZnO, a modified scheme was proposed where an onsite term U on Zn-d orbital was incorporated within the GW_0 framework. Additionally, a higher level of self-consistent scGW and the use of hybrid Heyd–Scuseria–Ernzerhof (HSE06) functional[33] to calculate wave functions and eigenvalues as starting conditions for G_0W_0 calculations were observed to overestimate the bandgap value. Pure DFT calculations employing LDA or GGA functionals predict a metallic state for InN.[11,23] Kumar et al.[29] utilized DFT + U to calculate the starting wave function, successfully introducing an optical gap in the electron structure of InN, enabling a more accurate representation of its behavior.

In this article, various GW approximation schemes were tested on GaN and InN to assess their validity and accuracy. A crucial consideration was to minimize the computational time required for electronic structure calculations, given the extraordinarily high demand for computing resources in studying the $In_xGa_{1-x}N$ ternary systems. With careful theoretical considerations, the optimal computational method was employed to accurately calculate the bandgap energy for the $In_xGa_{1-x}N$ ternary alloy. The electronic structure in $In_xGa_{1-x}N$ ternary alloys was investigated using $2 \times 2 \times 2$ supercells containing 32 atoms, considering concentrations of 25%, 50%, and 75% indium atoms to approximate a random alloy.[11]

To obtain the initial calculations, all numerical calculations were performed using HSE06, PBE,[34] and LDA functionals with the projector augmented wave (PAW) method which is an improved version of the pseudopotential method that partly accounts for the rapid oscillations of the wavefunction near the nucleus.[35] GW PAW pseudopotentials were employed in all calculations. These calculations were executed using the Vienna Ab initio Simulation Package.[36,37] The atomic structures of both InN and GaN were modeled using a fully relaxed wurtzite structure containing 4 atoms (C46v-P63mc: space group number 186).[38,39] The In-4d and Ga-3d electrons were treated as valence electrons. The electronic wave functions were described using a plane-wave basis set with an energy cutoff of 600 eV. k-point meshes of $6 \times 6 \times 6$ were utilized throughout the calculations to ensure well-converged results for GaN and InN. DFT calculations predicted a metallic state for InN. To open the optical bandgap, additional onsite correlation U in the Dudarev parameterization[40] was applied to In-3d states, with a U value of 3.5 eV. The total number of electronic bands was set to 1224 in order to conduct GW calculations using model supercells containing 32 atoms.

Duan et al.[23] demonstrated that theoretical bandgap values depend on cutoff energies and k-space partitions. Convergence of the calculated bandgap energy was observed at a cutoff energy of 600 eV. Notably, selecting a $4 \times 4 \times 4$ k-point mesh led to a 1.5% difference in calculated fundamental bandgap values compared with a $6 \times 6 \times 6$ mesh. Hence, the present numerical calculations were performed using a $2 \times 2 \times 2$ k-point mesh for this reason.

© 2024 The Author(s). physica status solidi (b) basic solid state physics published by Wiley-VCH GmbH

15213951, 2025, 3, Downloaded from https://onlinelibrary.wiley.com/doi/10.1002/pssb.202400107 by L.N. Gumilyov Eurasian National University, Wiley Online Library on [18/09/2025]. See the Terms and Conditions (https://onlinelibrary.wiley.com/terms-and-conditions) on Wiley Online Library for rules of use; OA articles are governed by the applicable Creative Commons License

15213951, 2025, 3, Downloaded from https://onlinelibrary.wiley.com/doi/10.1002/pssb.202400107 by L.N. Gumilyov Eurasian National University, Wiley Online Library on [18/09/2025]. See the Terms and Conditions (https://onlinelibrary.wiley.com/terms-and-conditions) on Wiley Online Library for rules of use; OA articles are governed by the applicable Creative Commons License

From the theoretical point of view, state-of-the-art calculations within many-body perturbation theory allow to rigorously obtain bandgap energy values. The GW approximation method used to compute self-energy corrections is a quite well-established and standard technique, giving energy levels generally in good agreement with experiments, even for complicated systems like reconstructed surfaces and clusters.[41] Due to the high complexity and large computational requirements of ab initio calculations of the self-energy, this approach has rarely been used to study systems with a large number of atoms in a unit cell. In the present study, the investigation of the $In_xGa_{1-x}N$ ternary alloy to estimate the bandgap value in the entire composition range with GW approximation was performed, predicting its properties without any experimental/fitting parameters.

Previous studies of $In_xGa_{1-x}N$ ternary alloy showed poor agreement of the DFT bandgap values with experimental data.[11,24,42–46] To improve consistency between theory and experiment, hybrid functionals in DFT have been used as an empirical simulation method. In the case of zinc-blende $In_xGa_{1-x}N$ ternary alloys, the overestimation of the bandgap energy in the In-rich region was found.[47] For AlN, GaN, and InN with wurtzite structure, the resulting bandgap values depend on the mixing ratio of the exact exchange energy functional. The mixing ratio is required to match the experimental bandgap energies increases with experimental bandgap energies.[11]

2.2. Summary of the Previous Results with the Present Calculation

To address the challenge of accurately describing the bandgap energy in the $In_xGa_{1-x}N$ ternary alloy system, it is crucial to select a suitable theoretical method that can equally and precisely capture the characteristics of both GaN and InN compounds. Reviewing the existing literature on InN and GaN, **Table 1** summarizes GW bandgap calculations. Notably, it is surprising to observe that only one study in the literature has demonstrated that the optimized effective potential (OEP) calculations effectively predict both lattice geometry and bandgap energy for both InN and GaN.[12] Unfortunately, the OEP method demands extensive computational resources, making it impractical to study large model cells, as required in the present research on ternary alloys. Given this limitation, we explored various approaches as initial stages to GW calculations within the framework of GGA, LDA, and hybrid functionals.

In addition to selecting the initial wave function for calculating GW energies and wavefunctions, which involves choosing the appropriate density functional, the geometric structure of the model cells significantly influences the theoretical values of the bandgap energy. The lattice constants of $In_xGa_{1-x}N$ ternary alloys can be determined through theoretical calculations, considering both lattice optimization and the use of interpolation formulae if the lattice parameters adhere to Vegard's laws. Another potential source of calculation errors arises from the challenge of conducting structural optimization within the real calculation process using the GW method.

In this study, unlike ref. [12], which relied on experimental values for lattice constants, we explore various functionals with a focus on their accuracy in predicting the geometry of the unit cells.

Table 1. Summary of the literature available on high-accuracy calculations of fundamental bandgap energy in InN and GaN with wurtzite structure.

Compound	Bandgap energy [eV]	Method (based on the WF obtained with this method)	Reference
InN	0.71	GW_0 + RPA (HSE3)	[26]
	0.99	scGW (LDA)	[27]
	0.74	Hybrid approach	–
	0.66	HSE06	[11]
	0.58	LDA with SIC[b]	[24,25]
	0.74	Simplified Gc[c]	–
	1.50	GW SIC (LDA)	–
	0.82	GW SIC (LDA)	[28]
	0.8	$scGW_0$	[29]
	0.7 (0.8 correction factor was applied)	GW + RPA (LDA)	[30]
	0.638, 0.765; 0.494[d]	G_0W_0 + SOC[e] (HSE)	[32]
	0.711	HSE06	[23]
	0.694	G_0W_0 (HSE06)	–
	0.805	$scGW_0$	–
	0.7	OEPx6 + G_0W_0 (LDA)	[12]
	0.0	PBE	[13]
	0.5	HSE06	[13]
	0.95	LDA-1/2	[21]
GaN	3.5	GW	[31]
	3.23	HSE06	[11]
	3.81 3.42	scGW (LDA) Hybrid approach[a]	[27]
	3.6 (0.8 correction factor was applied)	GW + RPA (LDA)	[30]
	3.659; 3.847; 3.366[d]	G_0W_0 + SOC[e] (HSE)	[32]
	3.24	OEPx[f] + G_0W_0 (LDA)	[12]
	3.52	LDA-1/2	[21]

[a]Combines 80% of the GW self-energy with 20% of the LDA self-energy as it is described in ref. [57]; [b]Self-interaction corrections; [c]Quasiparticle corrections to DFT within a simplified GW approximation; [d]Data obtained for geometries optimized using different methods (AM05, LDA, PBE); [e]Spin-orbit coupling; [f]Exact-exchange OEP.

The lattice geometry determined through this approach is then utilized for GW calculations, incorporating initial wave functions obtained from different functionals. The functional that yields the closest agreement between calculated bandgap values and experimental data is selected for further calculations, utilizing a model supercell of $In_xGa_{1-x}N$ ($x = 0.5$) ternary alloy with lattice constants calculated according to Vegard's law for comparison.

3. Results and Discussion

The results of the present numerical calculations on the lattice parameters in GaN and InN, in comparison with the experimental data, are provided in **Table 2**. The obtained data are characteristic of calculations performed by DFT. For InN, the hybrid

© 2024 The Author(s). physica status solidi (b) basic solid state physics published by Wiley-VCH GmbH

Table 2. The equilibrium values of the lattice constants for InN and GaN at atmospheric pressure calculated by various methods in comparison with experimental data. Parentheses indicate the relative error of calculations. The experimental values of lattice parameters for InN were obtained at $T = 105$ K.

Compound	*a* [Å] (error, %)	*c* [Å] (error, %)	Unit cell volume [Å^3]	*c*/*a*	*u*	Method
InN	3.5356	5.7005	61.710	1.6121	0.3773	Exp.[38]
	3.530 (−0.16)	5.700 (0.01)	61.52	1.614	0.379	HSE06
	3.578 (1.2)	5.777 (1.3)	64.06	1.614	0.379	PBE
	3.503 (0.9)	5.655 (0.8)	60.09	1.614	0.379	LDA
	3.62	5.83	–	1.61	–	PBE/HSE06[13]
GaN	3.19	5.28	46.53	1.655	0.375	Exp.[57]
	3.176 (−0.4)	5.173 (−2.0)	45.20	1.628	0.377	HSE06
	3.214 (0.8)	5.235 (0.9)	46.84	1.628	0.377	PBE
	3.156 (−1.1)	5.140 (−2.7)	44.34	1.628	0.377	LDA

functional predicts nearly exact lattice-constant values, whereas the PBE functional tends to overestimate, and the LDA functional overestimates parameter "*a*" and underestimates "*c*." In the case of GaN, the most accurate values for lattice constants are obtained using the PBE functional, while the HSE06 and LDA functionals underestimate these parameters. Thus, none of the selected methods for optimizing the crystal lattice is deemed preferable compared with experimental data for both considered compounds.

Additionally, all obtained equilibrium lattice geometries were utilized to calculate the bandgap values. For each structure, three possible wave functions served as the starting values for the numerical calculations within the bandgap energy values in GW approximation. The results are shown in **Table 3**. From these data, it is evident that only two approaches yield sufficiently accurate values with an error of less than 0.1 eV for both InN and GaN. These approaches are as follows: (case 1) $scGW_0$ approach with optimized geometry by HSE06 and starting wave functions by LDA, and (case 2) GW_0 calculations with LDA for both geometry optimization and starting wave functions.

Thus, two theoretical approaches yield approximately similar values for both the lattice geometry and the bandgap in both InN and GaN under study. Additionally, concerning the calculated values of the cell parameters, the use of the hybrid functional is somewhat closer to experimental values.[48] However, incorporating Hartree–Fock exchange in the hybrid functional significantly escalates computation costs, particularly with plane-wave basis sets.[49,50] Furthermore, for an accurate prediction of the bandgap width, the $scGW_0$ method is employed. This method involves an additional self-consistency procedure compared with GW_0, significantly increasing computational costs. Therefore, considering the balance between the predictive ability and required computational costs, LDA for structure optimization and wave functions calculation for GW_0 were employed in this study. In the latter case, the LDA + U method was applied to indium atoms, as indicated in Section 2. The summarized calculation procedure is illustrated in **Figure 1**.

The estimated lattice-constant values for the $In_xGa_{1-x}N$ ternary alloy, as a function of x, are depicted in **Figure 2**. The present numerical calculations were conducted for a $2 \times 2 \times 2$ supercell, which is eight times larger than the unit cell. The obtained data were then recalculated and presented as lattice constants for the unit cell. In creating the model structures, for $x = 0.25$ and 0.5, the substitution of gallium atoms was executed in a manner that ensured a uniform distribution of indium atoms throughout the cell, while avoiding both the clustering of indium atoms and their ordering, which could lead to the emergence of periodic superstructures. Previous results indicate

Table 3. The values of the bandgap for nitrides, calculated using various methods. The values that most closely coincide with the experimental values for both considered compounds are highlighted in bold.

Compound	Input geometry	Input wavefunction	Bandgap calculation method			
			DFT	G_0W_0	GW_0	$scGW_0$
			Bandgap [eV]			
1	2	3	4			
InN	HSE06	HSE06	0.76	**0.71**	0.71	0.89
		PBE + U	0.09	0.21	0.27	0.50
		LDA + U	0.11	0.43	0.51	**0.73**
	PBE	HSE06	0.60	0.49	0.48	0.66
		PBE + U	0.04	0.07	0.30	0.30
		LDA + U	0.03	0.14	0.14	0.40
	LDA	HSE06	0.85	2.65	2.59	2.63
		PBE + U	0.16	0.29	0.36	0.25
		LDA + U	0.26	**0.67**	**0.76**	0.94
GaN	HSE06	HSE06	**3.30**	3.77	3.85	3.97
		PBE	1.97	3.13	3.33	3.50
		LDA	1.99	3.16	3.38	**3.44**
	PBE	HSE06	3.02	3.47	3.67	3.67
		PBE	1.73	4.66	5.00	5.26
		LDA	3.03	**3.47**	3.57	3.63
	LDA	HSE06	3.46	3.93	4.01	4.14
		PBE	2.10	3.29	**3.51**	3.74
		LDA	2.12	3.33	**3.55**	3.69

© 2024 The Author(s). physica status solidi (b) basic solid state physics published by Wiley-VCH GmbH

15213951, 2025, 3, Downloaded from https://onlinelibrary.wiley.com/doi/10.1002/pssb.202400107 by L.N. Gumilyov Eurasian National University, Wiley Online Library on [18/09/2025]. See the Terms and Conditions (https://onlinelibrary.wiley.com/terms-and-conditions) on Wiley Online Library for rules of use; OA articles are governed by the applicable Creative Commons License

15213951, 2025, 3, Downloaded from https://onlinelibrary.wiley.com/doi/10.1002/pssb.202400107 by L.N. Gumilyov Eurasian National University, Wiley Online Library on [18/09/2025]. See the Terms and Conditions (https://onlinelibrary.wiley.com/terms-and-conditions) on Wiley Online Library for rules of use; OA articles are governed by the applicable Creative Commons License

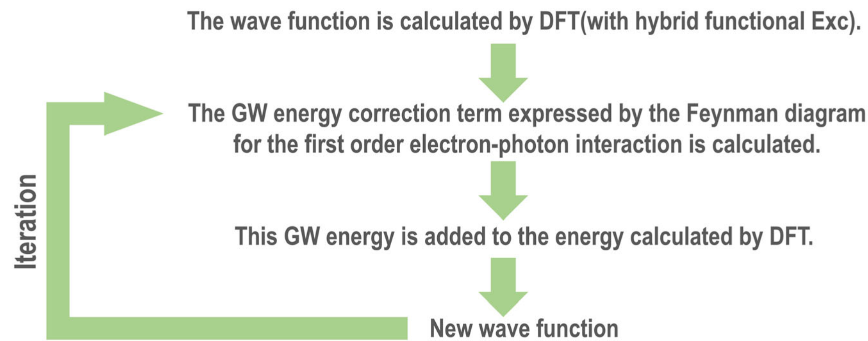

Figure 1. Calculation procedure of bandgap energy.

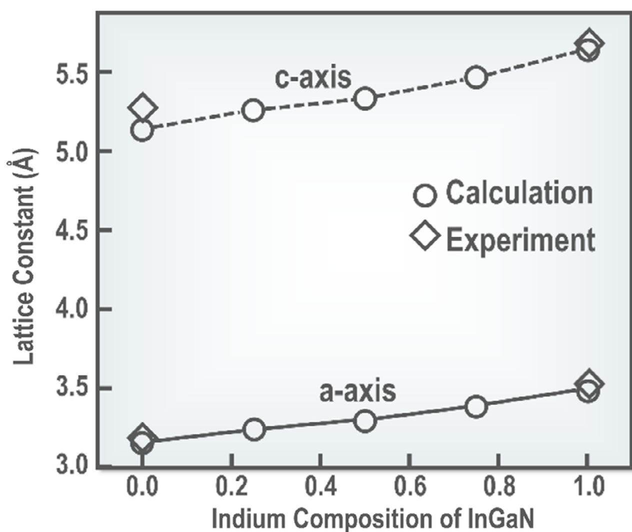

Figure 2. Numerically estimated lattice parameters of $In_xGa_{1-x}N$ within LDA in comparison with experimental values.[37,57]

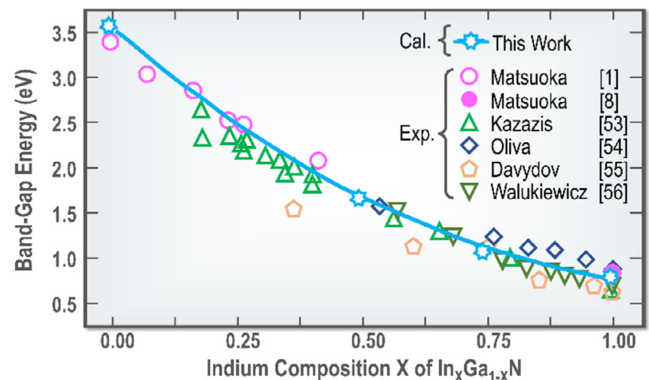

Figure 3. Theoretical and experimental values of the fundamental bandgap energy in $In_xGa_{1-x}N$ ternary alloy as a function of the indium molar fraction. Theoretical results are obtained using the GW_0 method (this work), HSE06 hybrid functional,[11] and LDA-1/2 method.[20] The bandgap energy GW (VL) value was obtained for a model cell with lattice constants calculated using Vegard's law. Experimental values are adopted from refs. [1,8,56,58–60].

that the clustering of $In_xGa_{1-x}N$ ternary alloy results in a more pronounced curvature of the bandgap energy dependence on the x value.[51] For the case $x = 0.75$, it is identical to $x = 0.25$ except for the mutual permutation of indium and gallium atoms. Test calculations on three different supercells with $x = 0.5$ demonstrated a weak (<2%) dependence of the bandgap energy on the choice of the atomic configuration. The geometries of all supercells were optimized, involving both the positions of the ions inside the supercells and the volume of the supercells. In this process, the lattice constants changed to ensure that the volume of the optimized cell corresponded to the system at zero external pressure, while maintaining constant lattice symmetry.

The linear dependence of cell parameters on indium content, as per Vegard's law, is evident. Atomic structures derived from this relationship were utilized to compute the bandgap energy, employing initial wave functions obtained through the LDA functional. **Figure 3** showcases the obtained data, comparing it with experimental data and prior calculations using the hybrid HSE06 functional.[11] Remarkably, our theoretical results, devoid of any parameters, align excellently with the experimental findings.

Additionally, we explored the impact of the model cell's starting geometry on the theoretical bandgap energy. This suggests that the lattice constants vary with the concentration of In and Ga Vegard's law. The calculated bandgap energy for the composition $In_{0.5}Ga_{0.5}N$ ternary alloy, employing GW calculations based on the LDA functional, is 1.36 eV. Notably, this value is 0.29 eV lower than the corresponding value obtained for a structure with theoretically determined lattice constants.

The bandgap energy in $In_xGa_{1-x}N$, varying with indium content, holds crucial significance for analyzing and designing efficient electronic devices. Qualitatively, there is a consensus that the bandgap energy in $In_xGa_{1-x}N$ exhibits a nonlinear relationship with the alloy composition. Traditionally, values of alloy bandgap energy are conventionally expressed as

$$E_g(In_xGa_{1-x}N) = (1-x)E_g(GaN) + xE_g(InN) - bx(1-x) \quad (2)$$

where b is the so-called bowing parameter. The semiconductor alloy system's most crucial parameter is the bandgap energy, and its departure from linear dependence is characterized by the bandgap bowing parameter "b," typically a function of

© 2024 The Author(s). physica status solidi (b) basic solid state physics published by Wiley-VCH GmbH

concentration. Several studies[24,42,45,51–54] have presented conflicting perspectives on the magnitude and indium concentration dependence of this bowing parameter. Some assert that a composition-independent bowing parameter does not accurately describe the bowing parameter.[11,24,42,52,55] Wu et al. utilizing optical absorption and photoluminescence measurements, proposed a constant bowing parameter of 1.4 eV for the bandgap energy versus composition is well described by [9]. In contrast, McCluskey et al. determined a bowing parameter value of 2.6 eV through optical absorption spectroscopy measurements.[51] Kazazis et al., through their measurement, suggested a bowing parameter value of 1.66 ± 0.08 eV adequately describes the intrinsic bandgap value dependency on the indium content across the entire range.[56] Our numerical results, obtained through a single-parameter bowing calculation expressed in Equation (2), yielded a value of $b = 1.85$ eV, with a maximum absolute error of less than 0.04 eV. This aligns well with the most recent experiment conducted by Kazazis et al.

Further exploration by Moses et al. demonstrated that the bowing parameter varies with indium concentration, decreasing with an increase in indium content.[11] While our results confirm this trend, they indicate a much lesser extent, providing b values of 1.92, 1.85, and 1.79 eV for 25%, 50%, and 75% of the indium content, respectively.

Up to now, $In_xGa_{1-x}N$ is only discussed; additionally, the other ternary alloys of $Ga_{1-x}Al_xN$ and $In_{1-x}Al_xN$ among InGaAlN system are also important for the device design. Test calculations have shown that for Al-containing Böelle alloys, the scGW0 method using PBE-optimized geometries and PDE input wavefunction provides more accurate predictions. Theoretical and experimental values of the fundamental bandgap energy in ternary alloys of $Ga_{1-x}Al_xN$ and $In_{1-x}Al_xN$ as a function of aluminum are shown in **Figure 4**a,b, respectively.

There is a common trend following the only physical parameter which we can compare with the experimental data of the bandgap value. Since the PBE method for $Ga_{1-x}Al_xN$ and $In_{1-x}Al_xN$ provides better agreement, one can expect that all other results are in better agreement as well. The exception is for $In_xGa_{1-x}N$ alloys. As shown in Table 3, in this case, the LDA method is more accurate. For the bandgap energy of InN, mutual compensation may occur. PBE functional overestimates lattice parameters, while LDA underestimates. This leads to a larger underestimation of the bandgap energy for PBE

Table 4. Bowing parameters b for $Ga_{1-x}Al_xN$ and $In_{1-x}Al_xN$ calculated by methods of G_0W_0, GW_0, and $scGW_0$.

Compound	b [eV]	Method
$Al_xGa_{1-x}N$	0.601	G_0W_0
	0.974	GW_0
	−0.927	$scGW_0$
$Al_xIn_{1-x}N$	2.280	G_0W_0
	2.2571	GW_0
	1.254	$scGW_0$

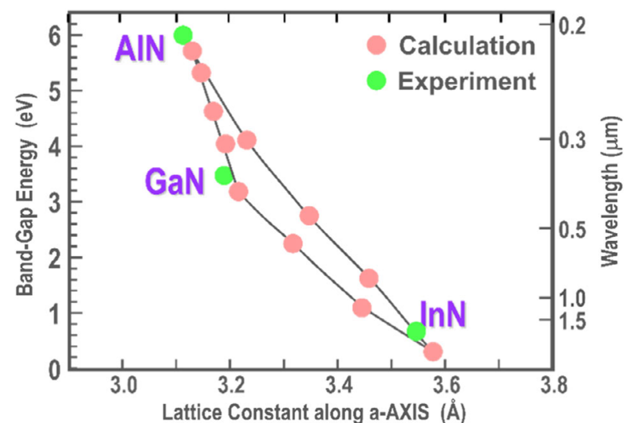

Figure 5. Relation between the fundamental bandgap energy and lattice-constant along a-axis calculated using the self-consistent GW_0 method with PBE in InGaAlN.

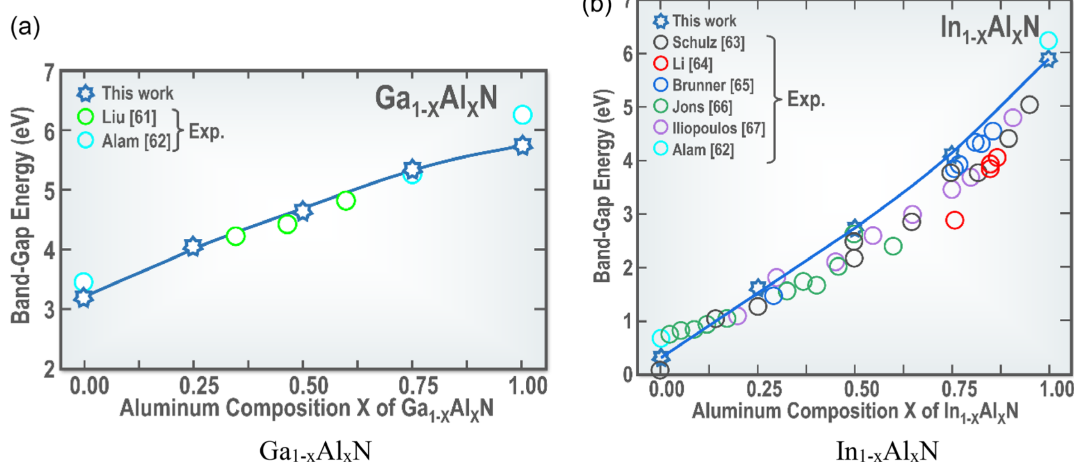

Figure 4. Theoretical and experimental values of the fundamental band-gap energy in ternary alloys of a) $Ga_{1-x}Al_xN$ and b) $In_{1-x}Al_xN$ as a function of aluminum. Theoretical results of this work are obtained using self-consistent GW_0 method with PBE. Experimental values are adopted from refs. [61–67].

© 2024 The Author(s). physica status solidi (b) basic solid state physics published by Wiley-VCH GmbH

15213951, 2025, 3, Downloaded from https://onlinelibrary.wiley.com/doi/10.1002/pssb.202400107 by L.N. Gumilyov Eurasian National University, Wiley Online Library on [18/09/2025]. See the Terms and Conditions (https://onlinelibrary.wiley.com/terms-and-conditions) on Wiley Online Library for rules of use; OA articles are governed by the applicable Creative Commons License

15213951, 2025, 3, Downloaded from https://onlinelibrary.wiley.com/doi/10.1002/pssb.202400107 by L.N. Gumilyov Eurasian National University, Wiley Online Library on [18/09/2025]. See the Terms and Conditions (https://onlinelibrary.wiley.com/terms-and-conditions) on Wiley Online Library for rules of use; OA articles are governed by the applicable Creative Commons License

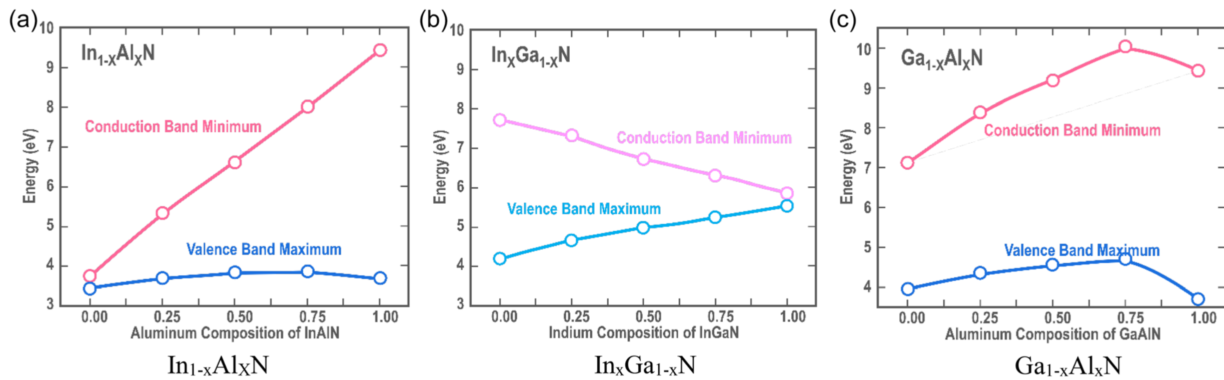

Figure 6. Energies of CBM and VBM of a) $In_xGa_{1-x}N$ and b) $In_{1-x}Al_xN$ calculated using self-consistent GW_0 method with PBE and c) $Ga_{1-x}Al_xN$ calculated using self-consistent GW_0 method with LDA.

compared with LDA. The bandgap energy calculated with LDA and PBE is 0.26 and 0.04, respectively. On the other hand, the spread of the bandgap energy values also depends on the initial wave function choice. The better agreement obtained between the LDA data and the experimental data may be considered to be largely due to chance. There may be more fundamental reasons for this, but we cannot immediately point them out.

Next, bowing parameters b for $Ga_{1-x}Al_xN$ and $In_{1-x}Al_xN$ calculated by methods of G_0W_0, GW_0, and $scGW_0$ are shown in **Table 4**.

The relation between the bandgap energy and the lattice constant along a-axis of InGaAlN is shown in **Figure 5** with experimental data of binary termination materials as the figure[1] first proposed by Matsuoka in 1990.

So far, only the bandgap energies have been discussed. For designing the devices such as optical devices with heterostructures, the barrier height at the connection in each valence band and the conduction band between both layers consisting of a heterostructure is also important. In the double heterostructure, each difference in the valence band and the conduction band plays a role as the barrier for hole and electron, respectively. The larger the barrier, the higher the luminous efficiency. Therefore, it is meaningful to show the dependence of the CBM and the VBM on the ternary alloy composition for $In_xGa_{1-x}N$, $In_{1-x}Al_xN$, and $Ga_{1-x}Al_xN$. All the data comes from the process of calculating bandgap energy. **Figure 6** shows the CBM and VBM of $In_xGa_{1-x}N$, $In_{1-x}Al_xN$, and $Ga_{1-x}Al_xN$ as a function of the composition of these materials. Figure 6a,b was calculated using self-consistent GW_0 method with PBE for $In_xGa_{1-x}N$ and $In_{1-x}Al_xN$, while the self-consistent GW_0 method with LDA was used for $Ga_{1-x}Al_xN$, consistent with the approach applied in the bandgap energy calculations mentioned earlier.

4. Conclusions

To address the challenge of determining bandgap values in ternary $In_xGa_{1-x}N$ alloys without relying on phenomenological parameters, various functionals have undergone preliminary testing. These tests encompass the optimization of model cell geometry and the calculation of initial wave functions for GW calculations applied to binary nitrides. Achieving acceptable accuracy for both InN and GaN involves the GW_0 approximation with LDA or the $scGW_0$ method with the hybrid HSE06 functional. Notably, successful reproduction of the narrow bandgap in InN has been accomplished without resorting to the phenomenological parameters.

Using LDA alone leads to a negative estimate of the bandgap energy in InN, indicating a metallic nature. To rectify this and induce a bandgap, the LDA + U method becomes necessary, albeit introducing a phenomenological parameter (U). Given its lower computational costs, the theoretical investigations on ternary $In_xGa_{1-x}N$ alloy presented here employ LDA with GW_0. The results demonstrate a robust agreement between theoretical predictions and experimental data. Additionally, it is observed that zone bending in this alloy can be effectively approximated using a quadratic function with a constant parameter, independent of x, set at 1.85 eV. This value closely aligns with the recent experimental findings.

After various discussions in this article, the bandgap energies of $In_xGa_{1-x}N$, $In_{1-x}Al_xN$, and $Ga_{1-x}Al_xN$ were successfully calculated without any parameters. The dependence of their bandgap energies on compositions was also calculated. It was also confirmed that the results almost reproduce the experimental values. Furthermore, the composition dependence of the difference between the CBM and VBM in the layers consisting of the double heterostructure, which is essential for configurations such as light-emitting devices and photodiodes, was also determined. The composition dependence of the bandgap values and the band discontinuity values between layers in double heterostructures presented in this article will be very useful for device design.

Acknowledgements

The authors are grateful to the JHPCN project as "jh190019-NAJ" at Research Institute for Information Technology Kyushu University, the High-Performance Computing Infrastructure (HPCI) (Project IDs hp220064, hp230037, and hp230468), and GIMR project as "202312-SCKXX-0510" at Center for Computational Materials Science, Institute for Materials Research, Tohoku University, for their continuous support of the supercomputing systems to be used for our simulation works. Y.K., one of the authors, is supported by Suranaree University of

© 2024 The Author(s). physica status solidi (b) basic solid state physics published by Wiley-VCH GmbH

Technology (SUT), Thailand Science Research and Innovation (TSRI), and the National Science, Research and Innovation Fund (NSRF). The work of T.M.I. was carried out within the state assignment of the Vernadsky Institute of Geochemistry and Analytical Chemistry of the Russian Academy of Sciences (GEOKHI RAS).

Conflict of Interest

The authors declare no conflict of interest.

Data Availability Statement

The data that support the findings of this study are available from the corresponding author upon reasonable request.

Keywords

bandgap energies, Green-function vertex approximation, InGaAlN, nitride semiconductors, theories

Received: February 23, 2024
Revised: October 31, 2024
Published online: November 28, 2024

[1] T. Matsuoka, H. Tanaka, T. Sasaki, A. Katsui, *Inst. Phys. Conf. Ser.* **1990**, *106*, 141.
[2] H. Amano, M. Kito, K. Hiramatsu, I. Akasaki, *Jpn. J. Appl. Phys.* **1989**, *28*, L2112.
[3] S. Nakamura, S. Senoh, T. Mukai, *Jpn. J. Appl. Phys.* **1993**, *32*, L83.
[4] Y. Shimizu, N. Banno, Japanese Patent, 2927279, **1996**.
[5] R. Haitz, J. Y. Tsao, *Phys. Status Solidi A* **2011**, *208*, 17.
[6] K. Prasertsuk, T. Tanikawa, T. Kimura, S. Kuboya, T. Suemitsu, T. Matsuoka, *Appl. Phys. Express* **2018**, *11*, 015503.
[7] a) N. Puchevrier, M. Menoret, *Thin Film Solids* **1976**, *36*, 141; b) C. O. Foley, T. L. Tansley, *Appl. Surf. Sci.* **1985**, *22/23*, 663.
[8] T. Matsuoka, H. Okamoto, M. Nakao, H. Harima, E. Kurimoto, *Appl. Phys. Lett.* **2002**, *81*, 1246.
[9] J. Wu, W. Walukiewicz, K. M. Yu, J. W. Ager III, E. E. Haller, H. Lu, W. J. Schaff, Y. Saito, Y. Nanishi, *Appl. Phys. Lett.* **2002**, *80*, 3967.
[10] V. Y. Davydov, A. A. Klochikhin, R. P. Seisyan, V. V. Emtsev, S. V. Ivanov, F. Bechstedt, J. Furthmu Èller, H. Harima, A. V. Mudryi, J. Aderhold, O. Semchinova, J. Graul, *Phys. Status Solidi B* **2002**, *229*, R1.
[11] P. G. Moses, M. Miao, Q. Yan, C. G. Van de Walle, *J. Chem. Phys.* **2011**, *134*, 084703.
[12] P. Rinke, M. Winkelnkemper, A. Qteish, D. Bimberg, J. Neugebauer, M. Scheffler, *Phys. Rev. B* **2008**, *77*, 075202.
[13] D. Liang, R. Quhe, Y. Chen, L. Wu, Q. Wang, P. Guan, S. Wangef, P. Lu, *RSC Adv.* **2017**, *7*, 42455.
[14] T. M. Inerbaev, T. Matsuoka, Y. Kawazoe, *Bull. Univ. Karaganda-Phys.* **2022**, *105*, 107.
[15] P. Hohenberg, W. Kohn, *Phys. Rev. B* **1964**, *136*, 864.
[16] Y. Kang, G. Kang, H.-H. Nahm, S.-H. Cho, Y. S. Park, S. Han, *Phys. Rev. B* **2014**, *89*, 165130.
[17] A. Rani, R. Kumar, *J. Supercond. Novel Magn.* **2017**, *30*, 1483.
[18] M. S. Hybertsen, S. G. Louie, *Phys. Rev. B* **1986**, *34*, 5390.
[19] F. Bechstedt, in *Plenary Lectures of the Divisions of the German Physical Society (DPG)*, Springer, Berlin **1992**, p. 177.
[20] R. R. Pelá, C. Caetano, M. Marques, L. G. Ferreira, J. Furthmüller, L. K. Teles, *Appl. Phys. Lett.* **2011**, *98*, 151907.
[21] L. G. Ferreira, M. Marques, L. K. Teles, *Phys. Rev. B* **2008**, *78*, 125116.
[22] L. Hedin, S. Lundqvist, in *Solid State Physics*, Vol. *23*, Academic Press, Cambridge **1969**, pp. 1–181.
[23] Y.-F. Duan, L.-X. Qin, L.-W. Shi, G. Tang, *Comput. Mater. Sci.* **2015**, *101*, 56.
[24] F. Bechstedt, J. Furthmüller, M. Ferhat, L. K. Teles, L. M. R. Scolfaro, J. R. Leite, V. Y. Davydov, O. Ambacher, R. Goldhahn, *Phys. Status Solidi A* **2003**, *195*, 628.
[25] F. Bechstedt, J. Furthmuller, *J. Cryst. Growth* **2002**, *246*, 315.
[26] L. F. J. Piper, L. Colakerol, T. Learmonth, P.-A. Glans, K. E. Smith, F. Fuchs, J. Furthmüller, F. Bechstedt, T.-C. Chen, T. D. Moustakas, J.-H. Guo, *Phys. Rev. B* **2007**, *76*, 245204.
[27] A. Svane, N. E. Christensen, I. Gorczyca, M. van Schilfgaarde, A. N. Chantis, T. Kotani, *Phys. Rev. B* **2010**, *82*, 115102.
[28] J. Furthmüller, P. H. Hahn, F. Fuchs, F. Bechstedt, *Phys. Rev. B* **2005**, *72*, 205106.
[29] M. Kumar, G. Baldissera, C. Persson, D. G. F. David, M. V. S. da Silva, J. A. Freitas, J. G. Tischler, J. F. D. Chubaci, M. Matsuoka, A. Ferreira da Silva, *J. Cryst. Growth* **2014**, *403*, 124.
[30] A. Punya, W. R. L. Lambrecht, *Phys. Rev. B* **2012**, *85*, 195147.
[31] A. Rubio, J. L. Corkill, M. L. Cohen, E. L. Shirley, S. G. Louie, *Phys. Rev. B* **1993**, *48*, 11810.
[32] L. C. de Carvalho, A. Schleife, F. Bechstedt, *Phys. Rev. B* **2011**, *84*, 195105.
[33] J. Heyd, G. E. Scuseria, M. Ernzerhof, *J. Chem. Phys.* **2006**, *124*, 219906.
[34] G. J. Paier, R. Hirschl, M. Marsman, G. Kresse, *J. Chem. Phys.* **2005**, *122*, 234102.
[35] P. E. Blöchl, *Phys. Rev. B* **1994**, *50*, 17953.
[36] G. Kresse, J. Furthmüller, *Phys. Rev. B* **1996**, *54*, 11169.
[37] G. Kresse, D. Joubert, *Phys. Rev. B* **1999**, *59*, 1758.
[38] W. Paszkowicz, R. ČernÝ, S. Krukowski, *Powder Diffr.* **2003**, *18*, 114.
[39] K. H. Hellwege, O. Madelung, in *Numerical Data and Functional Relationships in Science and Technology*, Springer, New York **1982**, p. 342.
[40] S. L. Dudarev, G. A. Botton, S. Y. Savrasov, C. J. Humphreys, A. P. Sutton, *Phys. Rev. B* **1998**, *57*, 1505.
[41] F. Aryasetiawan, O. Gunnarsson, *Rep. Prog. Phys.* **1998**, *67*, 237.
[42] M. Ferhat, F. Bechstedt, *Phys. Rev. B* **2002**, *65*, 75213.
[43] L. Bellaiche, T. Mattila, L.-W. Wang, S.-H. Wei, A. Zunger, *Appl. Phys. Lett.* **1999**, *74*, 1842.
[44] A. F. Wright, K. Leung, M. van Schilfgaarde, *Appl. Phys. Lett.* **2001**, *78*, 189.
[45] L. K. Teles, J. Furthmuller, M. R. Scolfaro, J. R. Leite, F. Bechstedt, *Phys. Rev. B* **2000**, *62*, 2475.
[46] K. Kim, W. R. L. Lambrecht, B. Segall, *Phys. Rev. B* **1997**, *53*, 16310.
[47] X. Wu, E. J. Walter, A. M. Rappe, R. Car, A. Selloni, *Phys. Rev. B* **2009**, *80*, 115201.
[48] J. Hafner, *J. Comput. Chem.* **2008**, *29*, 2044.
[49] M. Marsman, J. Paier, A. Stroppa, G. Kresse, *J. Phys. Condens. Matter.* **2008**, *20*, 64201.
[50] A. N. Chantis, M. van Schilfgaarde, T. Kotani, *Phys. Rev. Lett.* **2006**, *97*, 039903.
[51] I. Gorczyca, S. P. Lepkowski, T. Suski, N. E. Christensen, A. Svane, *Phys. Rev. B* **2009**, *80*, 075202.
[52] M. D. McCluskey, C. G. Van de Walle, L. T. Romano, B. S. Krusor, N. M. Johnson, *J. Appl. Phys.* **2003**, *93*, 4340.
[53] C. Caetano, L. K. Teles, M. Marques, A. Dal Pino Jr., L. G. Ferreira, *Phys. Rev. B* **2006**, *74*, 045215.
[54] I. Gorczyca, T. Suski, N. E. Christensen, A. Svane, *Appl. Phys. Lett.* **2010**, *96*, 101907.

© 2024 The Author(s). physica status solidi (b) basic solid state physics published by Wiley-VCH GmbH

15213951, 2025, 3, Downloaded from https://onlinelibrary.wiley.com/doi/10.1002/pssb.202400107 by L.N. Gumilyov Eurasian National University, Wiley Online Library on [18/09/2025]. See the Terms and Conditions (https://onlinelibrary.wiley.com/terms-and-conditions) on Wiley Online Library for rules of use; OA articles are governed by the applicable Creative Commons License

[55] C. G. Van de Walle, M. D. McCluskey, C. P. Master, L. T. Romano, N. M. Johnson, *Mater. Sci. Eng. B* **1999**, *59*, 274.
[56] S. A. Kazazis, E. Papadomanolaki, M. Androulidaki, M. Kayambaki, E. Iliopoulos, *J. Appl. Phys.* **2018**, *123*, 125101.
[57] V. Petkov, M. Gateshki, J. Choi, E. G. Gillan, Y. Ren, *J. Mater. Chem.* **2005**, *15*, 4654.
[58] R. Oliva, S. J. Zelewski, Ł. Janicki, K. R. Gwóźdź, J. Serafińczuk, M. Rudziński, E. Özbay, R. Kudrawiec, *Semicond. Sci. Tech.* **2018**, *33*, 035007.
[59] V. Y. Davydov, A. A. Klochikhin, V. V. Emtsev, D. A. Kurdyukov, S. V. Ivanov, V. A. Vekshin, F. Bechstedt, J. Furthmüller, J. Aderhold, J. Graul, A. V. Mudryi, H. Harima, A. Hashimoto, A. Yamamoto, E. E. Haller, *Phys. Status Solidi B* **2002**, *234*, 787.
[60] W. Walukiewicza, S. X. Lia, J. Wu, K. M. Yu, J. W. Ager III, E. E. Hallera, H. Lu, *J. Cryst. Growth* **2004**, *269*, 119.
[61] Y. Liu, Q. X. Li, L. Y. Wan, B. Kucukgok, E. Ghafari, I. T. Ferguson, X. Zhang, S. Wang, Z. C. Feng, N. Lu, *Appl. Surf. Sci.* **2017**, *421*, 389.
[62] S. N. Alam, V. Z. Zubialevich, B. Ghafary, P. J. Parbrook, *Sci. Rep.* **2020**, *10*, 16205.
[63] S. Schulz, M. A. Caro, L.-T. Tan, P. J. Parbrook, R. W. Martin, E. P. O'Reilly, *Appl. Phys. Express* **2013**, *6*, 120101.
[64] J. Li, K. B. Nam, M. L. Nakarmi, J. Y. Lin, H. X. Jiang, P. Carrier, S. H. Wei, *Appl. Phys. Lett.* **2003**, *83*, 5163.
[65] D. Brunner, H. Angerer, E. Bustarret, F. Freudenberg, R. Höpler, R. Dimitrov, O. Ambacher, M. Stutzmann, *J. Appl. Phys.* **1997**, *82*, 5090.
[66] E. Jones, R. Broesler, K. M. Yu, J. W. Ager, E. E. Haller, W. Walukiewicz, X. Chen, W. J. Schaff, *J. Appl. Phys.* **2008**, *104*, 123501.
[67] E. Iliopoulos, A. Adikimenakis, C. Giesen, M. Heuken, A. Georgakilas, *Appl. Phys. Lett.* **2008**, *92*, 191907.

© 2024 The Author(s). physica status solidi (b) basic solid state physics published by Wiley-VCH GmbH

15213951, 2025, 3, Downloaded from https://onlinelibrary.wiley.com/doi/10.1002/pssb.202400107 by L.N. Gumilyov Eurasian National University, Wiley Online Library on [18/09/2025]. See the Terms and Conditions (https://onlinelibrary.wiley.com/terms-and-conditions) on Wiley Online Library for rules of use; OA articles are governed by the applicable Creative Commons License